RESEARCH PAPER

ATMOSPHERIC CORROSION BEHAVIOR OF HOT-DIP GALVANIZED AND CONTINUOUS GALVANIZED STEEL

Gökmen Sığırcık [1], Ömer Yıldırım [2], Tunç Tüken [1]*

[1]Chemistry Department, Faculty of Science and Letters, Çukurova University, 01330, Adana, Turkey
[2]BORÇELİK R&D, 16601, Gemlik-Bursa, Turkey

*Corresponding author: ttuken@cu.edu.tr, tel.: +90 322 3386081, Chemistry Department, Faculty of Science and Letters, Çukurova University, 01330, Adana, Turkey

ABSTRACT

Five years of outdoor atmospheric corrosion tests of hot dip galvanized steel samples were performed, for products of continuous galvanizing and after fabrication batch galvanizing processes. For the purpose of comparison between corrosion performances of these two different galvanizing process products, an industrial coastal area (Gemlik-Bursa/TURKEY) was chosen for outdoor testing, which fits into C4 type corrosive atmosphere definition, according to ISO 9223. Samples were studied in laboratory with accelerated salt spray exposure test and electrochemical methods. Corrosion products formed on exposed samples and cross section of coatings are analyzed by SEM. Lead is observed to change the corrosion characteristics of the coatings with change in constituents of environments. In saline electrolytes, alloying of lead is found to accelerate corrosion rate. This metal deposits as cluster on top layer of the galvanized coatings and acts as strong cathodes with respect to the zinc and accelerates the corrosion rate. It was determined that differences in dip and continuous galvanization processes cause dramatic differences in the elemental composition, morphology and regional hardness values of coatings. In the comparison of corrosion resistance, lower performance of the dip galvanized coating, although it is much thicker, has been shown due to the differences mentioned above.

Keywords: Atmospheric corrosion; hot-dip galvanization; continuous galvanization

INTRODUCTION

Corrosion performance of galvanized steel samples is mostly considered to have linear correlation with zinc layer coating thickness. For this purpose, generally, time to first maintenance is utilized as selection criteria, which is defined as the time to 5% rusting of the steel surface [1-3]. Generally, the consumers prefer to follow up a shortcut, choosing unnecessarily high thickness of zinc coating, for long lasting corrosion performance. Another point, the thickness of zinc layer is a function of many variables (the thickness and elemental composition of steel substrate, process time, bath composition etc.) involved during coating process and precise thickness control is another issue. In this context, the coating technique has vital importance, either continuous hot-dip galvanizing or after-fabrication batch hot-dip galvanizing.

In the dip galvanizing technique, the parts taken from steel coils in appropriate sizes are shaped first, and then their surfaces are galvanized by immersing them in molten zinc pot (460°C). Coating thicknesses are not a precisely controlled parameter in dip galvanizing technique [4-6]. The composition of the material to be coated automatically reaches a certain limit value depending on its geometry and dipping time. Batch hot-dip galvanized coating is a complete immersion process applied after all welding, shearing, cutting-drilling, and hole punching, all surfaces are protected from corrosion by zinc [7-9]. Silicon and phosphorous content in steel yield the customary shiny silver coating and other percentages result in matte gray coatings. Typically, hot dip galvanized samples exhibit bright and shiny, passivation applications may change into dull appearance, which is applied for longer atmospheric corrosion endurance and/or for preparation of painting or other value-added processes. Regardless, after a short period of time (approximately 6 months or less in most atmospheric exposure conditions) the galvanized steel will look the same, i.e. matte gray. Batch type hot dip galvanizing baths generally includes Pb, thus the resulting galvanizing layer includes certain amounts of Pb, and also some Zn-Fe phases are formed during the process. Addition of some metals (Sb, Pb, Cd, etc.) in to bath may improve workability, fluid dynamics of molten zinc; substrate surface wettability and appearance of zinc layer [10-13].

Continuous galvanizing offers precisely controlled coating thickness and quality, as the product exits molten zinc bath, high-pressure air knives are used to remove excess molten zinc, then the product is cooled and rolled into large coils before delivery to the end user for eventual fabrication (cutto-length and formed to be used in automotive body panels, appliances, roofing, etc.). For the continuous hot dipped galvanizing process, the coating consists of a thin Al-Fe alloy interphase layer close to the steel surface, little amount of aluminum oxide is also considered as a contribution to shiny appearance [14-16].

After exposure to corrosive atmosphere, analysis of corrosion products provides significant data about the corrosion mechanism and the influence of species present in the environment [17]. In most cases, the products of atmospheric corrosion of zinc are found to be hydroxide, oxides compounds of zinc, which also include various species (carbonate, chloride, sulfate etc.) from pollutants. The said corrosion products form a layer on the surface, which determine kinetics mechanism and further progress of corrosion. Efficient physical barrier proper-

ty may eliminate transportation of corrosive ions (species) underlying metallic substrate, hindering the anodic/cathodic reactions [18,19]. In presence of CO_2 as pollutant in the atmosphere, zinc hydroxyl carbonate $(Zn_5(OH)_6(CO_3)_2)$ is readily formed on the surface, which has greater protection efficiency than zinc hydroxide/zinc oxide $(Zn(OH)_2/ZnO)$ forms. This is generally attributed to its high stability, low solubility and compact structure. The presence of CO_2 is generally considered as a drawback, since it is responsible for acidic pH values in the liquid film formed on the surface. So, the level (dose) of CO_2 becomes more important, as well as the frequency of condensation (wet-dry cycles) occurring on the surface due to daily cyclic change in temperature and humidity. As the exposure time increases, diversification of corrosion products has been reported previously, $Zn_4(OH)_6SO_4$, $Zn_4Cl_2(OH)_4SO_4$, $Zn_5(OH)_8Cl_2 \cdot H_2O$, $NaZn_4Cl(OH)_6SO_4 \cdot 6H_2O$ like compounds. After prolonged exposure time in the marine atmospheric environment, $NaZn_4Cl(OH)_6SO_4 \cdot 6H_2O$ is the major compound on zinc surface, which is the final product of sequential series of reactions, with time. Even though to its dull appearance, this product was proved to have important corrosion protection under marine atmosphere [20-22].

This study is a part of a long lasting research study, where the atmospheric corrosion behavior has been investigated C4 type industrial coastal atmospheric corrosion environment, for zinc coated steel samples prepared by continuous hot-dip galvanizing and after-fabrication batch hot-dip galvanizing procedures. In this paper, we have presented the evaluation of corrosion test results for 5 years, focusing on the differences in elemental composition, microstructure and relevant mechanical properties, as well as thickness.

MATERIAL AND METHODS

2.1. Test environment

The field tests of galvanized steel samples were performed in the campus of BORUSAN, which located in Gemlik-Bursa/TURKEY. The said location is an industrial coastal area, at which environment has industrial pollution (steel, chemical production, thermal power and automobile industries). The test station was 5 meters away from the sea (Gemlik Harbour with the following coordinates: 40°24'49.7"N 29°05'23.8"E). The air quality was assessed with help of data obtained from the ministry of environment database, which indicated to 80-90 μg m^{-3} PM10 and SO_2 < 35 μg m^{-3} in most of an average year. So, the test environment classification of atmospheric corrosion test area fits into C4 type corrosive atmosphere definition, according to ISO 9223. The temperature, humidity values for the years of atmospheric corrosion exposure were given in supplementary files. The experiments were carried out for 5 years in between June 2014 and June 2019. The samples were placed at an angle of 45°, facing south and they were placed on exposure racks as recommended in ASTM G50 - 10(2015) Standard Practice for Conducting Atmospheric Corrosion Tests on Metals.

2.2. Surface and cross-sectional analysis

The samples taken from outdoor exposure environment, the surface was washed by deionized water to remove dirt and loosely adsorbed salts etc., and then the morphology was inspected with help of field emission scanning electron microscopy equipped with energy dispersive X-ray spectroscopy (SEM-EDS/Zeiss Gemini). To observe the cross-sections of the corroded specimens at different exposure times, the specimens were cut and buried into bakelite resin to protect the surface with corrosion products and then the inspected cross-section

area was polished with silicon carbide papers and diamond pastes, respectively. Finally, the samples were rinsed in ethanol and deionized water. Periodically taken samples were analyzed with SEM, for products formed on the exposed samples and cross section of the coatings. The measurement of Vickers hardness was carried out by Emcotest DuraScan 50 G5 micro hardness tester through the load of HV 0.01 kg with dwell time of 7 s.

2.3. Electrochemical testing

Conventional three electrodes experimental design was employed with flat panel galvanized steel was the working electrode, a saturated calomel electrode as the reference and graphite rod as auxiliary electrode. Electrochemical impedance spectroscopy (EIS) measurements were performed by application of a sinusoidal voltage of 10 mV at the open-circuit potential of the working electrode while changing its frequency from 0.01 Hz to 100 kHz. The obtained data were analyzed using the Gamry Interface 1000 Potentiostat/Galvanostat. The EIS data were fitted with constant-phase element (CPE) model to extract the impedance parameters. All electrochemical measurements were performed at the temperature of 25±1ºC. The potentiodynamic (PD) polarization data were recorded in arranges of −0.25 V to +0.25 V vs. open circuit potential with a constant scan rate of 10 mV min^{-1}. The EIS, cathodic and anodic polarization measurements were simultaneously performed on the samples, and three sets of close values data (variation of ±2.5%) were averaged and produced in the paper. For electrochemical testing, fresh galvanized steel samples were utilized in order to investigate corrosion kinetics of different galvanizing techniques' products, at the beginning. For this purpose, 0.05% NaCl (Merck) aqueous solution was utilized as the corrosive test environment.

2.4. Solution analysis

Elemental composition of the materials was determined via induced coupled plasma (ICP) by dissolving of the materials.

RESULTS AND DISCUSSION

Before corrosion tests, the galvanized steel samples were examined for their elemental composition and morphologies through cross sections. Because the studied samples were products of two different techniques; batch hot dip coated samples and pieces taken from continuously hot dip coated coils, from now on, these samples will be named as BHDG and CHDG, respectively. For this purpose, zinc layers of BHDG and CHDG samples were dissolved carefully, as described in BS EN 10346:2015. In this method, hydrochloric acid (HCl, ρ=1.19 g mL^{-1}) is utilized in presence of hexamethylenetetramine $(C_6H_{12}N_4)$ as the corrosion inhibitor to prevent dissolution of iron [23].

Then, the solutions were analyzed with ICP and results were presented in Table 1. In the case of CHDG samples, includes higher amount of Al, while the Fe content was quite higher in BHDG samples. During this type of galvanizing process, extra aluminum is added into molten zinc, to obtain ultra-thin Fe_2Al_5 layer on steel sheet. The said interphase layer enhances the adhesion strength of Zn layer, on steel. On the other hand, remarkably high amount of Pb is found in zinc layer produced by BHDG, this was also related to intentionally added lead in molten zinc pot, during the process. In traditional BHDG baths, lead is added to obtain molten lead layer at the bottom of pot, which offers uniform bottom heating and operational advantages, as well as positive impact on the aesthetic look

(shiny, spangle appearance) [24]. As a result, certain amount of lead will be dissolved in molten zinc and found in the final galvanized article. There is an increasing trend for restriction of lead content in zinc layer of galvanized steel articles, for example ROHS (Restriction of hazardous substances) legislations recommend 0.1% of lead content as the highest limit in hot dip galvanizing bath. However, the lead content is still very high in galvanizing industries, because there is not a tangible consensus on those restrictions, yet.

Table 1 The ICP analysis results of BHDG and CHDG samples.

Material	Al%	Cd%	Fe%	Ni%	Pb%	Sn%	Zn%
BHDG	0.02	0.00	3.41	0.03	0.20	0.03	96.31
CHDG	0.23	0.00	0.58	0.00	0.00	0.00	99.19

For better understanding the texture, elemental distribution and general morphology, SEM-EDS analysis was realized for the cross sections of BHDG and CHDG samples, **Fig. 1**. As expected, the film thickness value was not the same at all points of surface, therefore an average value could be given for both samples, 90-100 and 50-60 µm for BHDG and CHDG samples, respectively. In the case of BHDG sample, the zinc layer includes some micro cracks and micro pores and white colored spots indicating to presence of different type of metallic species as a separate phase. This outcome is related to different galvanizing process conditions, immersion time, bath composition, cooling rate, etc.
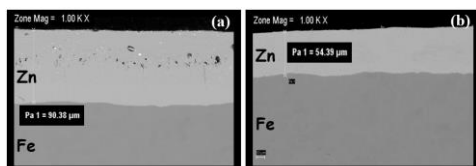
Fig. 1 The cross-section SEM views of BHDG (a) and CHDG (b) samples.

Fig. 2 shows EDS analysis data for Zn and Fe content through the cross sections of zinc layers. The formation of Fe_2Al_5 layer is clearly seen for CHDG sample, due to process, and this thin layer plays important role in adhesion and homogeneity of Zn layer on the steel substrate. Moreover, in the EDS line spectra analysis of CHDG sample, a peak was observed for Al content, during transition from substrate to galvanizing layer. This evidence was indicating to concentration of Al content in this region, as an interphase.

For further investigation, we have divided the galvanizing layers into 4 different zones (sections), beginning from the Fe/Zn interface to the top of coating layer. Then, distribution of Fe and Pb elements was analyzed for each section, shown in **Fig. 3** and the data was summarized in **Table 2**. Normally, the amount of Fe (w%) decreases gradually, from bottom to the top of galvanizing layers of both samples. The said iron content comes from the substrate, with diffusion Fe atoms through the freshly being formed Zn layer, in hot galvanizing bath. It was clear that BHDG process yields galvanizing layer with remarkably higher amount of iron, as well as lead content.

The presence of diverse elements has dramatic impact on mechanical, morphological and electrochemical properties of galvanizing layer. Lead content is more likely deposited as clusters at many places (white color in **Fig. 3**) of the coating. Even though there were small concentrations of aluminum, iron and silicon, the major component of these clusters was found to be lead. Moreover, there are similar results reported in

the literature, stating that the lead deposits preferably positioned in the η phase (the top layer) of zinc coating [25].
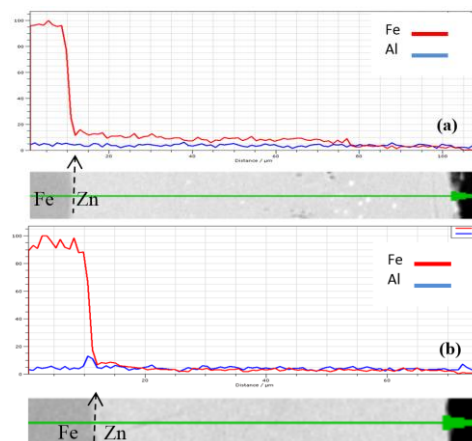
Fig. 2 The obtained line spectral EDS analysis results of BHDG (a) and CHDG (b) samples.
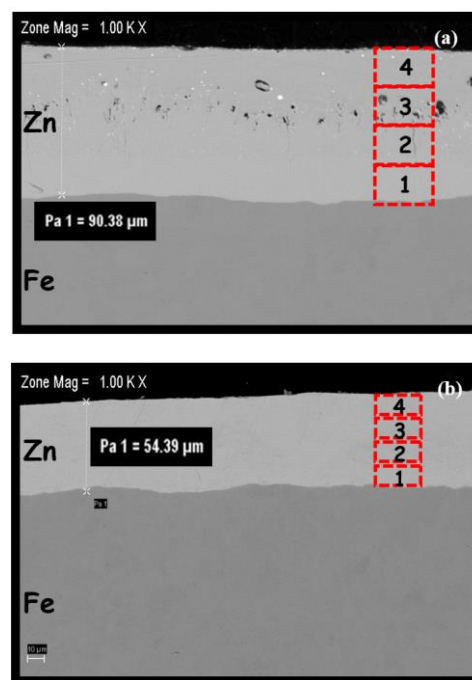
Fig. 3 The selected areas for cross sectional BHDG (a) and CHDG (b) samples from inside to the outside.

The clusters of lead stimulate formation of micro galvanic cells within the galvanizing layer, and deterioration is accelerated. Also, cross sectional inspection of BHDG sample clearly shows that there is serious number of defects within galvanizing layer, due to presence of considerably high amount of impurities (**Fig. 3**). Of course, the processing time and cooling

conditions are quite different and they may also have impact on this situation. The above findings were clear evidence for important differences between elemental composition and microstructure of two samples. Therefore, we have decided to measure the micro hardness values from different zones (sections) of galvanizing layers, from bottom to the top of cross sectional areas. The thicker galvanizing layer of BHDG (90-100 μm) allowed us to realize measurements from 5 different points on the cross section, the thickness of CHDG sample (50-60 μm) allowed for only 3 points. The obtained graphs are given in **Fig. 4**, plotting micro hardness value (Vickers) against the number indicating the test point. The micro hardness tests results along the cross side were summarized in Table 3 for BHDG and CHDG samples.

Table 2 The percentages of Fe and Pb for BHDG and CHDG samples from EDS data.

Material	Elements	Sections			
		1	2	3	4
BHDG	Fe%	8.86	6.90	1.93	1.20
	Pb%	-	-	-	2.91
CHDG	Fe%	1.78	1.04	0.77	0.70
	Pb%	-	-	-	-
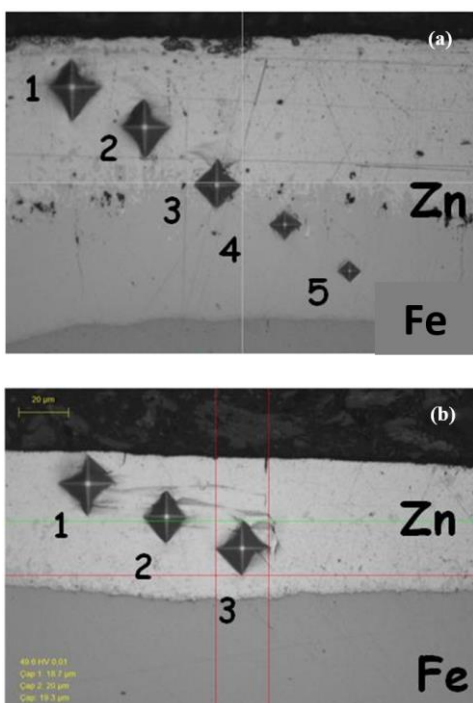
Fig. 4 Micro hardness test results along the cross side for BHDG (a) and CHDG (b) samples.

The hardness value changed dramatically along the cross section of BHDG sample's galvanizing layer, nearby the steel substrate it was 285 HV, decreased gradually and 50 HV was measured for the region near the top of coating (point 1). This situation was attributed to gradually changing iron content along the galvanizing layer, rather than the lead. Highest hardness value was measured near the steel substrate, where

the iron content was highest (8.86% by weight). The presence of iron increases the hardness value; moreover the hardness value decreases down to 42 HV on the top, where the iron content becomes 0.70% for CHDG sample. Then, the largest trace (indentation) was observed at point 1, after testing with square pyramidal diamond indenter. For galvanizing layer of the CHDG sample, micro hardness value changes very slightly (42-50 HV) starting from the steel/galvanizing layer interface through the top.

Table 3. Micro hardness tests results along the cross side for BHDG and CHDG samples.

Material	The measured area (HV)				
	1	2	3	4	5
BHDG	50	55	60	158	285
CHDG	42	47	50	-	-

3.2. Atmospheric Corrosion Testing Studies

Before exposure to atmospheric field, the sample surfaces were analyzed with SEM- EDS and the results are given in **Fig. 5**. From SEM images, the surface of BHDG was more likely homogenous, due to fact that there was Cr (III) passivation on the surface of CHDG sample. Cr (III) passivation process leaves a mixture deposit on the surface, where the major components are zinc oxide and chromium (III) oxide. Besides, the presence of oxide species was found on the surface of both samples, **Table 4**. In the case of BHDG sample, the galvanize layer surface is oxidized in the open atmosphere, readily.
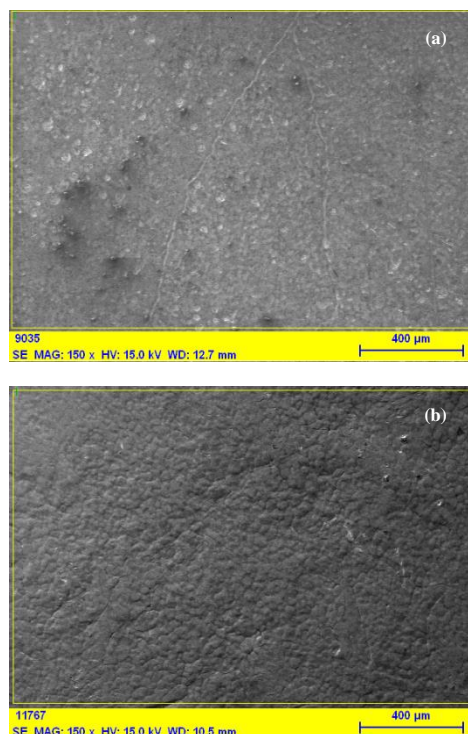
Fig. 5 SEM images of BHDG and CHDG samples prior to atmospheric corrosion tests.

Table 4 EDS results of BHDG and CHDG samples prior to atmospheric corrosion tests.

Material	Elements				
	Al%	Cr%	P%	O%	Zn%
BHDG	0.53	0.00	0.00	8.06	91.41
CHDG	0.64	1.05	0.74	2.73	94.84

The field tests have been started in the year of 2015, and small pieces were cut off from the main body and brought to laboratory for detailed analysis, in the following years, periodically. After cleaning the surfaces with ethanol and rinsing in water, dried samples were prepared for SEM analysis; recorded results are presented in **Figs. 6** and **7**. General appearance of surfaces changed with time, due to deposition of atmospheric corrosion products and co-deposition of some extra contaminations.
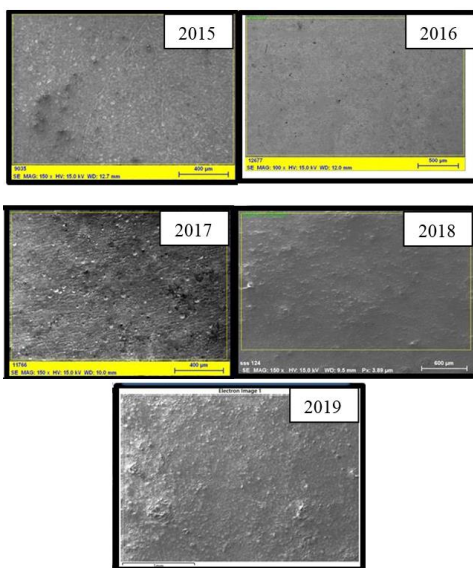
Fig. 6 SEM images of BHDG sample taken periodically for 5 years.
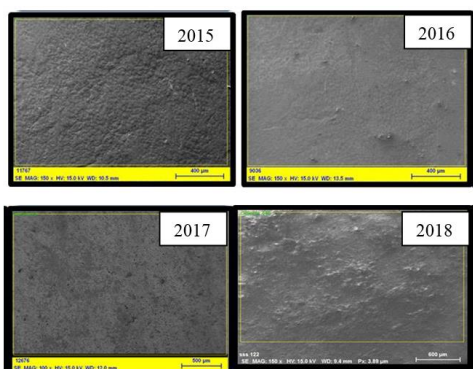
Fig. 7 SEM images of CHDG samples taken periodically for 5 years.

Within the humid layer on the surface, the following reactions take place where dissolved oxygen interacts with oxide and/or passive film free regions [26, 27].

Anodic Reaction: $Zn \rightarrow Zn^{2+} + 2e$ (1.)

Cathodic Reaction: $\frac{1}{2} O_2 + H_2O + 2e \rightarrow 2OH^-$ (2.)
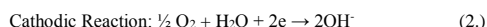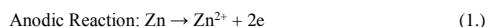
Depending on the dissolved atmospheric CO_2 and SO_x pollutants in industrial area and hydrolysis of freshly produced Zn^{2+} ions decrease the local pH value, nearby the surface. Thus, the reduction of H^+ ions could also take place as the cathodic reaction.

In **Tables 5** and **6**, the EDS analysis results are summarized for the samples exposed to industrial marine atmosphere, for 5 years. The percent amount of chloride (Cl^-), carbon (C) and sulphur (S) increased with time, since the atmospheric pollutants interact with the surface. While the presence of oxide deposits on the surface causes roughness, the moisture film formed by condensation on the surface increases these deposits. Atmospheric CO_2 dissolves in this moisture film and produces carbonate ion (CO_3^{2-}), which is readily deposited on the surface with various cations.

$CO_2 + H_2O \rightarrow H_2CO_3 \leftrightarrow H^+ + HCO_3^- \leftrightarrow 2H^+ + CO_3^{2-}$ (3.)
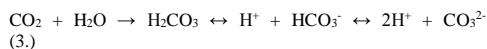
Firstly, $Zn(OH)_2$ which commonly known as white rust precipitates on the surface. In this stage, the proximity of the anode-cathode surfaces is very important. Because the Zn^{2+} cations released on the anode form a precipitate at the locally rising pH value with the release of OH^- anions on the cathode surface. This precipitate occurs quickly at pH > 8.4 and turns into ZnO which named as zincite. Since the cathodic reaction can also occur on the ZnO surface, whose electrical conductivity is higher compared to $Zn(OH)_2$, the cathodic surface area becomes wider. After prolonged exposure period, the continuity of zinc layer may disappear due to local corrosion or pitting, in these defective areas, the steel substrate interacts with the corrosive environment, and red rust appears on the surface. Nevertheless, within this story, there are numerous different sceneries, depending on the types and amount of pollutants in the atmosphere, as well as wet-dry cycle frequency.

As it was reported in many different research studies, chloride ions are able to react with freshly produced zinc hydroxide (white rust) to yield quite stable "hydroxychloride" compound (simonkolleite) on the surface. The following reaction generally accepted for this event [28].

$4ZnO + Zn^{2+} + 5H_2O + 2Cl^- \rightarrow Zn_5(OH)_8Cl_2 \cdot H_2O$ (4.)
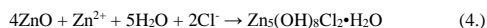
On the other hand, the carbonate (CO_3^{2-}) ions produced by dissolution of carbon dioxide in the atmosphere in water react with zinc hydroxide and form "hydrozincite" [29].

121

$$Zn(OH)_2 \ + \ 4Zn^{2+} \ + \ 4OH^- \ + \ 2CO_3^{2-} \ \rightarrow \ Zn_5(CO_3)_2(OH)_6$$
(5.)
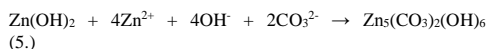
As a result of these formations, the surface gradually becomes dull and a color change process to gray takes place, on the surface.

Table 5 5 years EDS analysis results of BHDG sample.

Period (Year)	Elements								
	Al%	Si%	P%	S%	Fe%	C%	Cl%	Cr%	O%
0	0.53	-	-	-	-	-	-	-	8.06
1	0.65	1.11	-	2.15	0.48	1.90	0.45	-	15.14
2	0.74	1.25	-	2.53	1.06	2.23	0.55	-	27.70
3	0.80	1.75	-	3.17	1.17	3.94	0.59	-	26.63
4	1.49	1.81	-	1.57	1.26	4.88	0.23	-	32.75
5	1.91	1.95	-	1.91	1.38	3.96	0.38	-	32.73

Table 6 5 years EDS analysis results of CHDG sample.

Period (Year)	Elements								
	Al%	Si%	P%	S%	Fe%	C%	Cl%	Cr%	O%
0	0.64	-	0.74	-	-	-	-	1.05	2.73
1	1.28	0.31	0.62	0.56	0.31	1.51	0.24	0.61	6.29
2	1.76	0.42	0.59	1.38	0.47	1.80	0.46	0.72	13.55
3	1.49	1.14	0.51	1.21	0.74	1.03	0.56	0.72	18.02
4	1.60	1.20	0.36	1.25	0.91	4.21	0.24	0.64	25.15
5	1.81	1.37	0.33	1.26	1.03	3.53	0.29	0.52	30.70

For better understanding the severity of corrosion caused damage on galvanize layers and structure of corrosion products depositing on the surface, the samples were analyzed cross sectional. The SEM results are presented in **Figs. 8** and **9**, for the cross sections of BHDG and CHDG samples exposed to industrial marine atmosphere (C4 class). It was noted that 1 year exposure was sufficient for severe corrosion of thick galvanizing layer of BHDG sample. Highly porous and rough layer of corrosion products was detected on the surface, also, local severe damages were observed. Moreover, some lateral cracks were determined within the galvanizing layer of BHDG sample. The damaged areas due to local galvanic cells appeared to be white spots and/or pitting. As discussed previously (section 3.1.), the BHDG sample's galvanizing layer includes

significant amount of iron and lead. The bottom part of zinc layer is rich of iron, while the lead rich clusters are more likely to be found on the top. Typically, the galvanic cells occur between the lead rich clusters and zinc matrix, and then severe local corrosion damages occur, where the corrosive electrolyte solution can succeed to these parts.

Fig. 9 Cross-section SEM images of CHDG samples taken periodically for 5 years.

Fig. 8 Cross-section SEM images of BHDG samples taken periodically for 5 years.

We have previously shown that the iron content influence the micro hardness value dramatically, along the height of zinc layer. Therefore, this situation may cause those cracks either during forming process or stress cracking corrosion within the coating when the corrosive solution reaches to this region. It was noted that the formation of micro-cracks happen within the lower region of this type of galvanic layer, therefore it was

attributed to the elemental composition difference in the BHDG sample. In this thicker BHDG sample, 4-5 times greater hardness values were measured from top to bottom. Microstructural and elemental differences affect the formation of galvanic cells from the beginning of the corrosion event and accelerate corrosion rate. In this process, a more favorable environment is created for "local" and/or "pitting" corrosion.

The composition and surface properties were important for the corrosion products accumulating on the surface during atmospheric corrosion. Therefore, we have realized SEM-EDS analysis for 5th years exposed samples, after abrading the cross sections about 1 mm for three times. This kind of testing was thought to be necessary for making sure previously discussed happenings along cross sections. The obtained results were presented, layer by layer in **Figs. 10** and **11**, for BHDG and CHDG samples, respectively. By doing so, we have targeted to obtain convincing proofs for the way of corrosion progress through the zinc layers obtained by different techniques.

In the case of BHDG sample (**Fig. 11**), remarkable vertical cracks and deep caves due to corrosion were clearly seen. This situation is in well agreement with previously presented findings about separate phases of lead and micro galvanic cells, as well as micro defects present in BHDG sample. Once the corrosion starts over the surface, local corrosion cells may grove through the depths of galvanizing layer, due to elementally different regions from side to side. This scenario will certainly lead to formation of red rust on the surface with time. For the sample prepared with CHDG process, the surface is getting oxidized uniformly, due to limitedly soluble corrosion products of zinc are formed on the uniform galvanizing layer (**Fig. 11**).
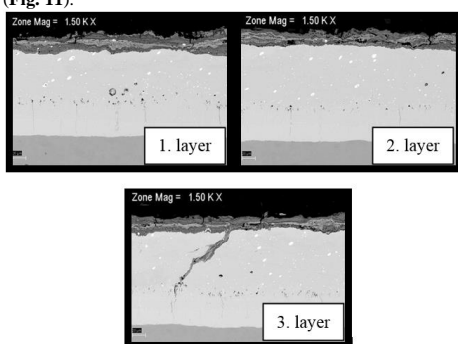
Fig. 10 SEM analysis into the interior of the BHDG sample along the z-axis after 5 years.
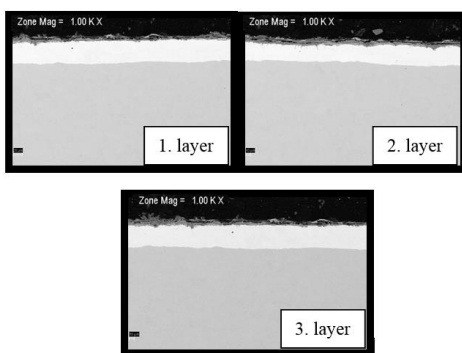
Fig. 11 SEM analysis into the interior of the CHDG sample along the z-axis after 5 years.

EDS mapping analysis was realized for better illustrating the situation difference between BHDG and CHDG samples, form cross section views, after 5 years, **Fig. 12**. Typically, pitting corrosion progressing through the BHDG sample's zinc layer is seen.

This time, the EDS mapping analysis of original (noncorroded) BHDG sample in order to explain the reasons for such severe cavitation risk, during atmospheric corrosion (**Fig. 13**). In the region close to the surface, it was clearly observed that corrosion process was intense around the lead micro particles (light blue) and the oxide corrosion products, green color surrounding the particle. Galvanic couple is formed when the corrosive solution penetrating down the surface (formed by the condensation of the humidity in the atmosphere and increasing its aggressiveness with the pollutants) reaches the part where the lead micro particle is located. This galvanic couple occurs in places where different types of metals coexist and are exposed to corrosive environment, enables corrosion to occur much faster [30]. When lead and zinc are present together, zinc (E°= -0.763 V) is much more active than lead (E°= -0.126 V).

For a more detailed analysis for oxide thickness change in BHDG and CHDG samples against the zinc loss due to corrosion, the cross-sectional analyses of the samples taken at the end of 5 years were given in **Fig. 14**. The thickness of the galvanized layer on the steel surface is not the same everywhere, depending on the underlying surface texture and other variables. Therefore, zinc thicknesses varying between 90-100 μm for BHDG sample and 50-60 μm for CHDG sample were measured before the atmospheric corrosion tests. It has been determined that the samples exposed to C4 class atmospheric corrosion for 5 years have decreased up to ~33 μm for BHDG. At the same time, the maximum thinning of the CHDG sample was around ~18 μm. As a result, the performance of the most risky region should be taken as a basis for red rust formation in a galvanized material.
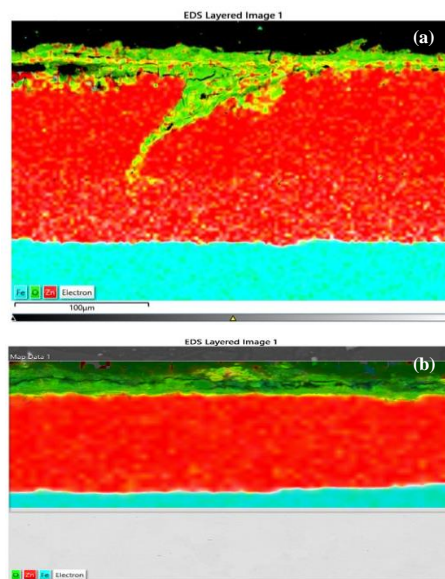
Fig. 12 EDS mapping analyzes for the cross sectional BHDG (a) and CHDG (b) samples achieved after 5 years.
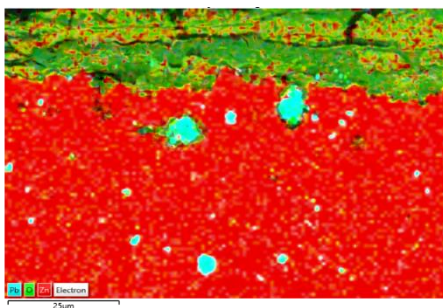
Fig. 13 The effect of Pb micro particles on corrosion of BHDG samples.
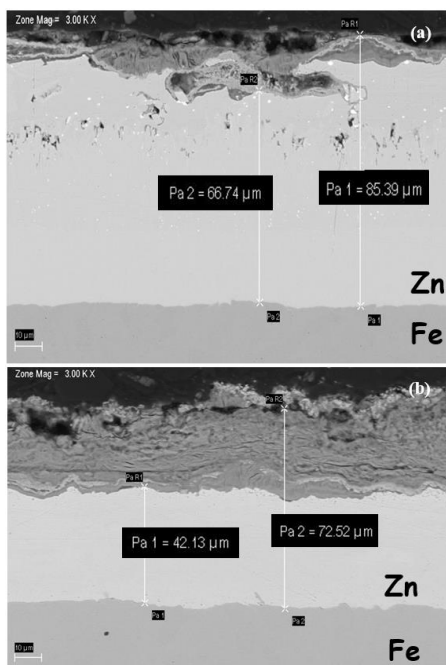
Fig. 14 Oxide films after 5 years atmospheric corrosion for BHDG (a) and CHDG (b) samples.

3.3. The electrochemical performance of the BHDG and CHDG samples

PD polarization measurements were carried out to investigate the corrosion behavior of BHDG and CHDG samples in 0.05% NaCl solution. PD polarization results recorded in the range of corrosion potential (E_{corr}) ± 250 mV were given in **Figs. 15a** and **b**. In these curves, the magnitude of the current flowing through the surface is directly dependent on the corrosion rate. The rate and current (as $\mu A\ cm^{-2}$) of corrosion were determined by analyzing the anodic (> E_{corr}) and/or cathodic (< E_{corr}) regions with the methods specified in the relevant standards. The magnitude of this current is directly proportional to the amount of material dissolved/oxidized by corrosion from the surface. Therefore, this method is used to quantitatively compare the corrosion performance of different types of materials [31]. At the end of only 0.5 hours, the corrosion current densities for BHDG and CHDG samples were determined as 40.5 and 7.2 $\mu A\ cm^{-2}$, respectively. It is seen that corrosion rate is 5-6 times faster on the BHDG sample surface.
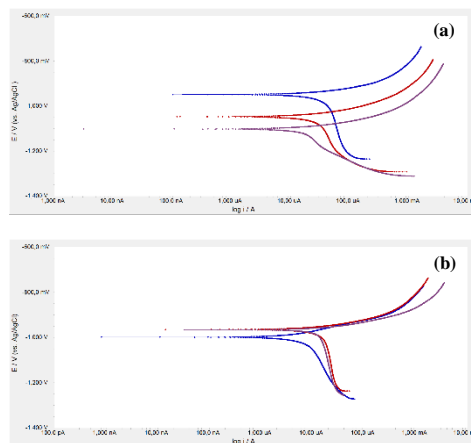
Fig. 15 PD polarization results for BHDG (a) and CHDG (b) samples obtained in 0.05% NaCl solution for 0.5h (blue), 24h (red) and 48h (purple) immersion time.

Over time, corrosion rates tend to decrease as corrosion products form on the surface of both materials. However, in any case the corrosion rate of the BHDG sample is always higher. This is the result of the elemental composition difference, micro particles and defects in the zinc coating of the BHDG sample, as discussed in the previous sections, increasing the corrosion rate. After 2 days, corrosion product deposits formed on the surfaces of the samples. $Zn(OH)_2$ deposit, which is the main corrosion product on the surface, has a limited stability ($K_{sp} = 1.8 \times 10^{-14}$) and while dissolving slowly, it moves away from the surface by diffusion and into solution. The dissolution of zinc, the formation of $Zn(OH)_2$ and its separation from the surface by dissolving determine the total corrosion rate. As these steps progress, corrosion rates that change day by day reach a stable value after a while. The corrosion current values were determined as 29.5 and 15.7 $\mu A\ cm^{-2}$ after 1 and 2 days for BHDG, respectively. Moreover, these corrosion current values were found as 11.6 and 13.2 $\mu A\ cm^{-2}$ after 1 and 2 days for CHDG, respectively. This result is consistent with the comparison results of oxide formation/zinc thinning rates obtained from cross-section SEM analyses in field samples and given in the previous sections.

EIS measurements were carried out and shown in Figs. 16a and b for BHDG and CHDG samples in 0.05% NaCl solution at different exposure period. From these EIS measurement results, changes of the oxide film on the surface over time and its permeability can be observed directly over the resistance values [32]. It is also seen from EIS results that the corrosion resistance of the passive oxide film on the surface of the CHDG sample, whose surface is zinc, coated with a thickness of 40-50 μm and passivized, is higher.

A small amount of newly formed oxide can better protect the surface with oxides that are the product of passivation previously applied to the surface. Although, more corrosion products form on the surface of BHDG sample with immersion time, they are far from being protective. The obtained EIS parameters were also presented in **Table 7**.
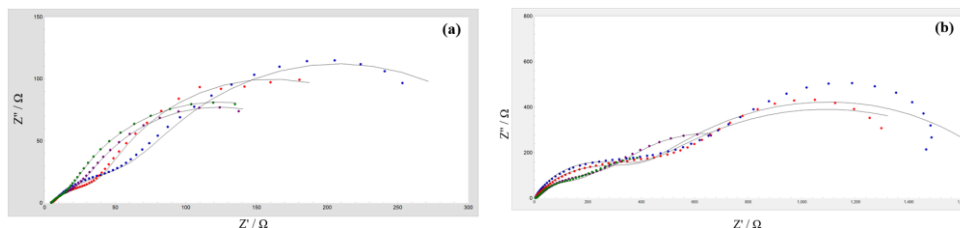
Fig. 16 EIS results for BHDG (a) and CHDG (b) samples obtained in 0.05% NaCl solution for 2.5h (blue), 7.5h (red), 24h (purple) and 48h (green) immersion time.

Table 7 Electrochemical parameters of BHDG and CHDG samples derived from EIS results.

Material	R1 (Ω)	CPE1 ($s^n \Omega^{-1}$)	n1	R2 (Ω)	CPE2 ($s^n \Omega^{-1}$)	n2	R3 (Ω)	CPE3 ($s^n \Omega^{-1}$)	n3
BHDG 2.5h	76.99	4.269×10^{-3}	0.53	271.3	21.87×10^{-3}	0.85	-	-	-
BHDG 7.5h	44.2	7.25×10^{-3}	0.53	232.5	39.12×10^{-3}	0.89	-	-	-
BHDG 24h	28.33	14.56×10^{-3}	0.55	187.4	47.62×10^{-3}	0.86	-	-	-
BHDG 48h	15.27	18.40×10^{-3}	0.58	210.5	41.89×10^{-3}	0.83	-	-	-
CHDG 2.5h	371.1	68.48×10^{-6}	0.76	1470	1.206×10^{-3}	0.66	-	-	-
CHDG 7.5h	370.2	177.8×10^{-6}	0.67	1087	2.341×10^{-3}	0.62	378.9	351.4×10^{-3}	0.62
CHDG 24h	303.6	1.596×10^{-3}	0.56	390.0	27.48×10^{-3}	0.22	334.2	14.19×10^{-3}	0.85
CHDG 48h	115.9	2.651×10^{-3}	0.77	150.6	25.15×10^{-3}	0.20	495.0	14.23×10^{-3}	0.69

CONCLUSIONS

The atmospheric corrosion performance of BHDG and CHDG samples were studied under C4 type corrosive atmospheric environment conditions for 5 years. The field test results were evaluated taking into account the differences between elemental compositions, microstructures, thickness, adhesion strength. The said differences naturally occur, since the galvanizing process involves dramatically different conditions. From aspect of practical applications, there are still serious considerations about selection criteria of these two types of galvanized steel products. In the case of CHDG samples, Al content is high, while the Fe content is much higher in BHDG samples.

The Fe content exhibits a gradually decreasing trend along the cross section of zinc coating, in BHDG. The high Al content of CHDG sample is attributed to intentionally added extra Al in molten bath, for the purpose of ultra-thin Fe_2Al_5 layer on steel substrate, which serves like an interphase enhancing the strength of adhesion. The high Fe content of BHDG samples, caused gradually changing hardness values, which was ranging between 50 and 285 HV, while the hardness value remains stable (~42 HV) through the zinc coating of CHDG sample. The said differences were shown to have great influence on corrosion progression within the years and the severity of damage. At the end of 1-year exposure in test field area, the surface of BHDG sample was covered with highly rough and porous corrosion products, with locally observed severe damages. Cross section analysis of corroded samples showed that lateral cracks occurred within the zinc layer. These results were attributed to locally differing composition and microstructure from side to side, within the product of BHDG process. After the onset of corrosion process on the surface, these local diversities provoke pitting, selective corrosion mechanisms and cracks formation.

SEM-EDS analysis of BHDG and CHDG samples, after 5 years' exposure to field testing, serious vertical cracks and deep caves were observed for BHDG sample. This situation is in well agreement with separate phases of lead and micro galvanic cells, as well as micro defects present in BHDG sample. This scenario will certainly lead to formation of red rust on the surface with exposure time. For the sample prepared with CHDG process, the surface is getting oxidized uniformly, due to limitedly soluble corrosion products of zinc are formed on the uniform galvanizing layer. From cross section analysis of these corroded samples, ~33 μm loss in thickness of zinc layer for BHDG, while this value was ~18 μm for CHDG.

Accelerated electrochemical test results corroborated previous results; moreover, for the first hours of exposure to 0.05% NaCl test solution, corrosion current densities were determined as 40.5 and 7.2 μA cm^{-2} for BHDG and CHDG samples, respectively. It is seen that corrosion rate is 5-6 times faster on the BHDG sample. The corrosion rates tend to decrease as corrosion products accumulate on the surface, with time. However, the kinetics and mechanism of corrosion on BHDG, lead much severe damage and always higher than CHDG.

As a conclusion, the thickness of galvanizing layer should not be taken as a guarantee for corrosion performance. Precisely controlled metallurgical properties, lead and iron content, thus the physical properties are much more important, when comparing the corrosion performance of BHDG and CHDG products, in practical applications under atmospheric conditions.

REFERENCES

1. N. Michailidis, F. Stergioudi, G. Maliaris, A. Tsouknidas, Influence of galvanization on the corrosion fatigue performance of high-strength steel, Surface & Coatings Technology, 259, 2014, 456-464.
https://doi.org/10.1016/j.surfcoat.2014.10.049.

2. P. Shreyas, Bijayani Panda, A.D. Vishwanatha, Characteristics of stainless steel-galvanized steel joint: Effect of stainless steel composition and welding parameters, Materials Today: Proceedings, 19, 2019, 468-473. https://doi.org/10.1016/j.matpr.2019.07.637.

3. V. Padilla, P. Ghods, A. Alfantazi, Effect of de-icing salts on the corrosion performance of galvanized steel in sulphate contaminated soil, Construction and Building Materials, 40, 2013, 908-918. https://doi.org/10.1016/j.conbuildmat.2012.09.077.

4. M. Blumenau, M. Norden, F. Friedel, K. Peters, Wetting force and contact angle measurements to evaluate the influence of zinc bath metallurgy on the galvanizability of high-manganese-alloyed steel, Surface & Coatings Technology, 205, 2010, 828-834. https://doi.org/10.1016/j.surfcoat.2010.07.123.

5. E.P. Najafabadi, Amin Heidarpour, Sudhir Rain, Hot-dip galvanizing of high and ultra-high strength thin-walled CHS steel tubes: Mechanical performance and coating characteristics, Thin-Walled Structures, 164, 2021, 107744. https://doi.org/10.1016/j.tws.2021.107744.

6. N. Gowripalan, H.M. Mohamed, Chloride-Ion Induced Corrosion of Galvanized and Ordinary Steel Reinforcement in High-Performance Concrete, Cement and Concrete Research, 28(8), 1998, 1119-1131. https://doi.org/10.1016/S0008-8846(98)00090-8.

7. A.P. Yadav, H. Katayama, K. Noda, H. Masuda, A. Nishikata, T. Tsuru, Effect of Fe–Zn alloy layer on the corrosion resistance of galvanized steel in chloride containing environments, Corrosion Science, 49, 2007, 3716-3731. https://doi.org/10.1016/j.corsci.2007.03.039.

8. T. Liang, H. Yuan, C. Li, S. Dong, C. Zhang, G. Cao, Y. Fan, X. Zhao, X. Cao, Corrosion inhibition effect of nano–SiO2 for galvanized steel superhydrophobic surface, Surface & Coatings Technology, 406, 2021 126673. https://doi.org/10.1016/j.surfcoat.2020.126673.

9. S.M. Mousavifard, M.M. Attar, A. Ghanbari, M. Dadgar, Application of artificial neural network and adaptive neuro-fuzzy inference system to investigate corrosion rate of zirconium-based nano-ceramic layer on galvanized steel in 3.5% NaCl solution, Journal of Alloys and Compounds 639, 2015, 315-324. https://doi.org/10.1016/j.jallcom.2015.03.052.

10. M.C. Fleming, *Solidification Processing*, 60, McGraw Hill Publishing, 1974, p. 36, 290-7.

11. R.E.R. Hill: *Physical Metallurgy Principles*, D. Van Nostrand Publishing Co., 1964, p. 47.

12. *Standard specification for steel sheet, zinc coated (galvanized) or zinc-iron alloy coated (Galvannealed) by the hot dip process*, ASTM A653/653M-19A.

13. H. Asgari, M.R. Toroghinejad, M.A. Golozar1, The Role of Texture and Microstructure in Optimizing the Corrosion Behaviour of Zinc Hot-dip Coated Steel Sheets, ISIJ International, 48 (2008) 628–633. https://doi.org/10.2355/isijinternational.48.628.

14. H. Kancharla, G.K. Mandal, S.S. Singh, K. Mondal, Effect of strip entry temperature on the interfacial layer and corrosion behavior of galvanized steel, Surface & Coatings Technology, 433 (2022) 128071. https://doi.org/10.1016/j.surfcoat.2021.128071.

15. D. Persson, D. Thierry, O. Karlsson, Corrosion and corrosion products of hot dipped galvanized steel during long term atmospheric exposure at different sites world-wide, Corrosion Science 126, 2017, 152-165. https://doi.org/10.1016/j.corsci.2017.06.025.

16. A. Azimi, F. Ashrafizadeh, M.R. Toroghinejad, F. Shahriari, Metallurgical assessment of critical defects in continuous hot dip galvanized steel sheets, Surface & Coatings Technology, 206, 2012, 4376-4383. https://doi.org/10.1016/j.surfcoat.2012.04.062.

17. A. Nazarova, M.G. Olivier, D. Thierry, SKP and FT-IR microscopy study of the paint corrosion de-adhesion from the surface of galvanized steel, Progress in Organic Coatings, 74, 2012, 356-364. https://doi.org/10.1016/j.porgcoat.2011.10.009.

18. C. Soriano, A. Alfantazi, Corrosion behavior of galvanized steel due to typical soil organics, Construction and Building Materials, 102, 2016, 904-912. https://doi.org/10.1016/j.conbuildmat.2015.11.009.

19. C. Qiao, L. Shen, L. Hao, X. Mu, J. Dong, W. Ke, J. Liu, B. Liu, Corrosion kinetics and patina evolution of galvanized steel in a simulated coastal-industrial atmosphere, Journal of Materials Science & Technology, 35, 2019, 2345-2356. https://doi.org/10.1016/j.jmst.2019.05.039.

20. E. Diler, B. Rouvellou, S. Rioual, B. Lescop, G.N. Vien, D. Thierry, Characterization of corrosion products of Zn and Zn–Mg–Al coated steel in a marine atmosphere, Corros. Sci., 87, 2014, 111-117. https://doi.org/10.1016/j.corsci.2014.06.017.

21. I. Odnevall, C. Leygraf, Formation of NaZn4Cl(OH)6SO4·6H2O in a marine atmosphere, Corros. Sci., 34, 1993, 1213-1229. https://doi.org/10.1016/0010-938X(93)90082-R.

22. I. Odnevall, C. Leygraf, W.W. Kirk, H.H. Lawson (Eds.), *Atmospheric Corrosion*, ASTM STP 1239, American Society for Testing of Materials, Philadelphia, 1995, pp. 215-229.

23. BS EN 10346:2015. *Continuously hot-dip coated steel flat products for cold forming - Technical delivery conditions*. The British Standards Institution 2015. Published by BSI Standards Limited 2015 ISBN 978 0 580 82407 4.

24. J.E. Spanier, R.D. Robinson, F. Zhang, S.W. Chan, I.P. Herman, Size-dependent properties of CeO2-y nanoparticles as studied by Raman scattering, Phys. Rev. B, 64, 2001, 245407. https://doi.org/10.1103/PhysRevB.64.245407.

25. S. Paswan, J.K. Singh, D.D.N. Singh, Effect of lead alloying on corrosion characteristics of galvanized coatings exposed in atmosphere, simulated laboratory and a service environment, Surfaces and Interfaces, 21, 2020, 100752. https://doi.org/10.1016/j.surfin.2020.100752.

26. D.A. Jones, N.R. Nair, Electrochemical Corrosion Studies on Zinc-Coated Steel, Corrosion, 41(6), 1985, 357-362. https://doi.org/10.5006/1.3582017.

27. R. Yıldız, İ. Dehri, Investigation of the cut-edge corrosion of organically-coated galvanized steel after accelerated atmospheric corrosion test, Arabian Journal of Chemistry, 8, 2015, 821-827. https://doi.org/10.1016/j.arabjc.2013.04.023.

28. S. Peng, S.K. Xie, F. Xiao, J.T. Lu, Corrosion behavior of spangle on a batch hot-dip galvanized Zn-0.05Al-0.2Sb coating in 3.5 wt.% NaCl solution, Corrosion Science, 163, 2020, 108237. https://doi.org/10.1016/j.corsci.2019.108237.

29. V. Padilla, A. Alfantazi, Corrosion film breakdown of galvanized steel in sulphate–chloride solutions, Construction and Building Materials 66 (2014) 447-457. https://doi.org/10.1016/j.conbuildmat.2014.05.053.

30. P.A. Kamble, P.P. Deshpande, S.T. Vagge, Numerical investigation of galvanic corrosion between galvanized steel and mild steel in bolted joint, Materials Today: Proceedings, 50, 2022, 1923-1929. https://doi.org/10.1016/j.matpr.2021.09.316.

31. G. Sığırcık, T. Tüken, M. Erbil, Assessment of the inhibition efficiency of 3,4-diaminobenzonitrileagainst the corrosion of steel, Corrosion Science, 102, 2016, 437-445. http://dx.doi.org/10.1016/j.corsci.2015.10.036.

32. E. Baran Aydın, G. Sığırcık, Preparations of different ZnO nanostructures on TiO2 nanotube via electrochemical method and its application in hydrogen production, International Journal of Hydrogen Energy, 44, 2019, 11488-11502. https://doi.org/10.1016/j.ijhydene.2019.03.123.